1 Title: Exploring the Lightning Jump Characteristics

2 Authors:

3 T. Chronis[1], L. D. Carey[1], C. J. Schultz[1,2], E. V. Schultz[1], K. M. Calhoun[3], and S. J.

4 Goodman[4]

5 [1] University of Alabama in Huntsville, Earth System Science Center

6 [2] NASA Marshal Space Flight Center

7 [3] Oklahoma University Cooperative Institute of Mesoscale Meteorology Studies,

8 National Severe Strom Laboratory,

9 [4] NOAA Satellite and Information Service (NESDIS)

10

11 Corresponding Author: Themis Chronis, themis.chronis@nsstc.uah.edu

12 University of Alabama in Huntsville

13 Earth System Science Center

14 320 Sparkman Dr., Huntsville 35805, AL

15

16

17

18

19

20

21

Abstract

This study is concerned with the characteristics of storms exhibiting an abrupt temporal increase in the total lightning flash rate (i.e., lightning jump, LJ). An automated storm tracking method is used to identify storm "clusters" and total lightning activity from three different lightning detection systems over Oklahoma, northern Alabama and Washington, D.C. On average and for different employed thresholds, the clusters that encompass at least one LJ (LJ1) last longer, relate to higher Maximum Expected Size of Hail, Vertical Integrated Liquid and lightning flash rates (area-normalized) than the clusters that did not exhibit any LJ (LJ0). The respective mean values for LJ1 (LJ0) clusters are 80 min (35 min), 14 mm (8 mm), 25 kg m^{-2} (18 kg m^{-2}) and 0.05 flash min^{-1} km^{-2} (0.01 flash min^{-1} km^{-2}). Furthermore, the LJ1 clusters are also characterized by slower decaying autocorrelation functions, a result that implies a less "random" behavior in the temporal flash rate evolution. In addition, the temporal occurrence of the last LJ provides an estimate of the time remaining to the storm's dissipation. Depending of the LJ strength (i.e., varying thresholds), these values typically range between 20-60 min, with stronger jumps indicating more time until storm decay. This study's results support the hypothesis that the LJ is a proxy for the storm's kinematic and microphysical state rather than a coincidental value.

1. **Introduction**

The advent of ground-based lightning detection networks in recent decades has made real-time retrieval of total lightning activity (cloud-to-ground, CG and the intra-

cloud, IC) available in both high spatial and temporal resolutions. Although there are uncertainties in the details (Takahashi 1978; Saunders 1993), it is known that rebounding collisions between graupel and ice crystals in the presence of super-cooled water is the primary process for thunderstorm electrification (MacGorman and Morgenstern 1998; Saunders et al. 2006; Emersic and Saunders 2010). Several studies have documented a temporal co-variability between updraft mass flux, precipitation ice mass and overall storm depth with the respective total lightning activity (e.g., Goodman et al. 1988; Carey and Rutledge 2000; Chronis et al. 2007; Deierling and Petersen 2008; Bruning and MacGorman 2013). Hence, it would be reasonable to suggest that an abrupt temporal change of the order of a few minutes in the total lightning activity is considered as a severe weather indicator ("Lightning Jump", LJ, see Schultz et al. 2009; 2011). Studies by Williams et al. (1999), Gatlin and Goodman (2010), Carey et al. (2009), Schultz et. al. (2009; 2011) and Rudlosky and Fuelberg (2013) document that statistics such as lead time, probability of detection and false alarm ratio could be improved based on the use of total lightning as a metric for storm intensity. Nonetheless, these methods can be hindered by problems related to uncertainties in severe weather observations at the surface (Trapp et al. 2006; Keene et al. 2008; Schultz et al. 2011). This study puts forward an original comparison between the convective characteristics of storms that did or did not exhibit a LJ throughout their lifetime. This evaluation relies on radar-derived and lightning properties.

2. Data and Methods

64   *2.1 Storm Tracking and Clustering*

65   The storm identification and tracking have been performed in real-time utilizing

66   the Warning Decision Support System Integrated Information tracking system (WDSS-

67   II, Lakshmanan et al. 2007). A storm "cluster" is automatically identified by the

68   reflectivity across the -10°C isothermal layer, following a merger of individual WSR-

69   88D radars.   A combination of watershed segmentation and k-means clustering is

70   employed to identify the storm clusters (Lakshmanan et al. 2009; Kolodziej Hobson et

71   al. 2012; Cintineo et al. 2014).   To complete the storm identification, the algorithm

72   searches for local reflectivity (Z) maxima where $Z > 20$ dBZ, then incrementally grows

73   the area until it is at least 200 km^2. The storm cluster is then matched with a separately

74   identified cluster at the next time step (for our analysis, a 1-min time step was used)

75   using a cost function, where longer-lived cells are given preference in the case of storm

76   mergers.

77   Each storm (hereinafter cluster) is described by a geolocated polygon (i.e.

78   footprint). The cluster's lifespan is determined as the total time a cluster was identified

79   and tracked by WDSS-II (Lakshmanan and Smith 2009). The Maximum Vertical

80   Integrated Liquid (VIL, Greene and Clark 1972) and the Maximum Expected Size of

81   Hail (MESH, Witt et al. 1998; Cintineo et al. 2012) are retrieved for each cluster for the

82   duration of its lifetime. Both VIL and MESH have been used as radar-derived intensity

83   metrics for storm properties such as liquid precipitation, updraft strength and hail growth

84   (Amburn and Wolf 1996; Witt et al. 1998). As with any proxy, there are caveats that

85   reflect the imperfect representations of severe weather potential and emanate from

86   parameters unrelated to the storm dynamics (e.g. distance from the radar, tilted updrafts,

87   storm speed etc., Stumpf et al. 2004). To mitigate these effects as much as possible, all

88   available radars in the area are used to retrieve these proxies. Five radars over each of

89   the three locations are employed, namely, KFDR, KTLX, KVNX, KINX, KSRX for

90   Oklahoma, KHTX, KGWX, KBMX, KDHX, KFFC for north Alabama and KLWX,

91   KDOX, KAKQ, KCCX, KDIX for DC (radar acronyms from

92   https://www.ncdc.noaa.gov/nexradinv/map.jsp). The data for the present study extends

93   from 1 April 2013 through 14 August 2013.

94   *2.2 Total Lightning Activity and the Lightning Jump Algorithm*

95   This study employs three total lightning detection networks: 1) the Lightning

96   Mapping Array (LMA) networks located in central/SW Oklahoma (MacGorman et al.

97   2008), North Alabama (Goodman et al. 2005), and Washington D.C (Krehbiel 2008) 2)

98   the Earth Networks Total Lightning Network (ENTLN, Liu and Heckman 2010) and 3)

99   the National Lightning Detection Network (NLDN, Cummins et al. 1995,2005,

100   Cummins and Murphy 2009).

101   The LMA networks detect the very high frequency (VHF) radiation emitted

102   during the elemental processes that compose a lightning discharge (e.g. the initial

103   breakdown, leader propagation and other K-processes, Uman 1987) with a location

104   accuracy measured in tens of meters and with a time resolution of 80-100 μs (Thomas et

105   al. 2004). The LMA detects both IC and CG flashes although the distinction can be

106   dubious due to limitations in range. The location accuracy is also range-dependent,

107   however it is relatively constant between ~150 km radius from the respective center

108   (Thomas et al. 2004; Koshak et al. 2004). The following analysis relies on the total

109   lightning flashes occurring within ~120 km of the respective LMA center (Thomas et al.

110   2003). Lightning flashes are retrieved from the LMAs via grouping at least 10 detected

111   VHF radiation sources, using time and space constraints (3 km and 150 ms) between the

112   adjoining points (McCaul et al. 2008). Only flashes that begin within the storm cluster's

113   footprint are counted towards the total flash rate. No classification between CG and IC

114   flashes is performed using LMA data.

115   The ENTLN sensors operate over a wide frequency range, spanning from 1 Hz to

116   12 MHz. According to Liu and Heckman (2011), electric field waveforms are used in

117   locating as well as classifying the IC and CG flashes. Multiple strokes (or individual

118   cloud events) are clustered into a single flash if they are within 700 ms and 10 km of the

119   first detected stroke. A flash that contains at least one return stroke is classified as a CG

120   flash, otherwise it is classified as an IC flash.

121   Since the late 1980s, the National Lightning Detection Network (NLDN,

122   Cummins et al. 1995; 1998; 2006) has served as the source for many CG lightning-

123   related studies over the US. The network consists of 113 sensors that combine the

124   advantages of direction finding and time-of-arrival techniques. The NLDN CG detection

125   efficiency ranges between 90-95% over the mid latitude continental US, with a median

126   location error better than 500 m (Cummins and Murphy 2009; Rudlosky and Fuelberg

127 2010). Although the NLDN is designed to primarily detect CG flashes, it has been

128 recently reported that IC flashes are also detected depending on the restrictions applied

129 to the processed waveforms (peak-to-zero rise time, Murphy and Nag, 2014).

130   The present study employs the total flash activity (IC+CG) for all lightning

131 detection systems. Rudlosky and Fuelberg (2013) use a similar methodology for

132 compiling lightning and radar data. Both NLDN and ENTLN have national (US)

133 coverage. Nevertheless, for this analysis the respective total lightning activity is

134 computed only for the clusters that are identified over a radius around where the

135 optimum LMA operation is ensured. Further detailed comparison (e.g., relative location

136 accuracy and detection efficiency) between the lightning detection systems lies outside

137 the scope of this paper. However, their employment is considered as a preliminary

138 attempt to demonstrate results pertaining to the LJ properties from lightning detection

139 networks of different technical specifications (e.g., detection efficiency).

140   The 1-min flash rate is computed by adding all the flashes occurring within the

141 footprint of the identified cluster. The LJ is objectively identified by Schultz et al. (2009;

142 2011). This technique uses 14 min of the cluster's most recent flash rate history. Twelve

143 of the 14 minutes are considered to calculate the minimum jump threshold that must be

144 exceeded for a LJ to occur. The remaining two minutes are used to determine whether

145 the current rate of change in the total flash rate exceeds the LJ threshold. As outlined in

146 Schultz et al. (2009; 2011), the algorithm is a 5-step process. These steps are as follows:

147 1) The total flash rate ($f\ min^{-1}$) from the 14 minute period is binned into two minute

148   segments and the total flash rate is averaged (Eqn. 1)

149   $FR_{avg}(t) = \frac{FR(t)+FR(t-1)}{2}(1)$

150   2) The rate of change of the total flash rate (DFRDT, f min^{-2}) is calculated by subtracting

151   consecutive bins from each other (Eqn. 2) $\frac{d}{dt}FR_{avg}(t) = \frac{FR_{avg}(t)-FR_{avg}(t-1)}{2} = DFRFT$

152   (2)

153   This results in six DFRDT values (f min^{-2}) 3) The five earliest DFRDT values in time

154   are used to calculate the standard deviation (σ) of the population 4) If DFRDT > α * σ

155   and the flash rate is in greater than a given flash rate threshold (FRT) then a LJ has

156   occurred. Note that -α- represents a multiplicative factor (i.e. dimensionless) and has no

157   relation to the standard deviation (σ). In the original studies by Schultz et al. (2009;

158   2011) α and FRT were set to 2.0 and 10 f m^{-1}. Also note that α is dimensionless (i.e., f

159   min^{-2} /f min^{-2}). Here we compute the LJ based on a variable α (0.5 - 4, step of 0.5) and

160   FRT (5-25 f m^{-1}, step of 5 f m^{-1}). The latter is employed in order to define the LJ relative

161   strength. For example, a weaker LJ1 would have α=1.0 and FRT=10 f m^{-1} while a

162   stronger LJ1 would be considered as α=2.0 and a FRT=15 f m^{-1} 5) This process is

163   repeated every two minutes as new total lightning flash rates are collected until the

164   storm dissipates.

165   We note that the above implemented time-window within which the LJ is

166   calculated is based on empirical observations of the growth and decay on the convective

167   time scale (<10-20 minutes). Had we allowed for longer periods (e.g. 40-60 minutes)

168   into the thunderstorm's lifetime we would likely have missed the occurrence of the first

169   LJ and potentially severe weather occurrence. This is why we've empirically tested this

170   algorithm with over 700 storms in multiple storm environments to help understand the

171   variability of the algorithm (Schultz et al. 2011). The choice of the $2*\sigma$ (i.e. $\alpha=2$) in

172   Schultz et al. (2011) is simply a benchmark to which this study is not tied to.

173   3. Analysis and Discussion

174   *3.1 Data and Quality control*

175   As WDSS-II tracks clusters independently of the respective total lightning

176   activity, the number of the identified LJ0 and LJ1 clusters is considerably different. For

177   instance more than 2,000 clusters are classified as LJ0 at $\alpha=2.0$ f m^{-2} and FRT=10 f m^{-1}

178   whereas less than 200 are classified as LJ1 for the same α and FRT values. To ensure a

179   comparable sample size and improve the representativeness of the data, we report on the

180   LJ0 and LJ1 clusters that exhibit sustained total lightning activity for more than 95%

181   during their lifespan (e.g., if a cluster is tracked for 100 minutes, the cluster must exhibit

182   total lightning activity greater than zero for at least 95 minutes). This quality constraint

183   (QC1) may classify a slightly different number of clusters depending on the employed

184   lightning detection system. An additional quality constraint (QC2) is applied to the

185   clusters that start or end at a flash rate that is notably higher than zero (set to >10 f m^{-1}).

186   Typically, these cases represent merging or splitting clusters or clusters that

187   entered/exited the effective radius of the LMA with high flash rates. QC2 also takes

188   care of potential problems with MESH/VIL repetitiveness due to distance from the

189 radar. Given that the study explores aspects such as the storm duration, the clusters that

190 failed to conform to QC2 are omitted from the analysis. Figure 1 illustrates examples

191 from a tracked cluster that exhibits a problematic tracking (e.g. cluster entering the area

192 with already high flash rates, Fig. 1a), a normal tracking (i.e. comply with both QC1 and

193 QC2, Fig. 1b), a LJ0 cluster (Fig. 1c) and a LJ1 cluster (Fig. 1d) of comparable flash

194 rates.

195 All three lightning detection systems indicate that the number of LJ1 clusters

196 decreases as the α and FRT values increase (i.e. fewer clusters at higher α and FRT

197 values, Fig. 2b, d, and f). Unlike the LJ1, the number of tracked LJ0 clusters increases as

198 the values of α and FRT increase (Fig. 2a, c, and e). The latter should be expected since

199 a LJ0 at e.g. α=2.0 and FRT=10 f m^{-1} will also not exhibit LJ at higher α or FRT values.

200 *3.2 The Autocorrelation function of LJ0 and LJ1 Flash Time Series.*

201 Autocorrelation is an essential tool for describing the independence of sequential

202 values in a time series. A slow (fast) decaying autocorrelation function with time (i.e.

203 lag) indicates a consistent (random) behavior of the variable under consideration

204 (Bowerman and O'Connell 1979). For example, a slow-decaying autocorrelation

205 function of lightning activity time-series would signal a coherent behavior in the storm's

206 updraft speed and volume (e.g., Schultz et. al. 2009; 2011; Schultz et al. 2014).

207 Consequently, autocorrelation can elaborate on whether the presence of a LJ relates to a

208 numerically random increase in the total lightning activity or points to a more persistent

209 feature of the storm's dynamical evolution. The autocorrelation function is computed for

210　　the flash rates of LJ0 and LJ1, by introducing a time lag that ranges from 1 to +N/2

211　　minutes, where N is the number of 1-minute intervals during which the cluster is tracked

212　　(i.e., lifespan). The lag at which the Pearson correlation is reduced below the 95%

213　　significance level denotes the "*e-folding*" time.. Figure 3 illustrates the average e-folding

214　　times for the LJ0 and LJ1 clusters for different α and FRT values. The corresponding

215　　results (Fig. 3) show longer e-folding times for the LJ1 clusters. For example, the e-

216　　folding times for the LJ1 at α=2.0 and FRT=15 f m^{-1} are computed as ~12 min for LMA,

217　　12.7 min for the ENTLN, and 11.5 min for the NLDN. Conversely, the e-folding times

218　　for the LJ0 for the same α and FRT values are consistently less than ~4.0 min for all

219　　three lightning detection systems and any given α and FRT value.　Moreover, the fact

220　　that the e-folding times for LJ1 clusters increase as both α and FRT values also increase,

221　　illustrates a key observation that emphasizes the non-redundant numerical role of both

222　　variables α and FRT in the LJ algorithmic implementation (Schultz et al. 2009; 2011).

223　　　　　*3.3 Comparison of storm severity potential and physical characteristics between*

224　　*the LJ0 and LJ1 clusters.*

225　　　　　The previous section studied the LJ0 and LJ1 clusters exclusively from the

226　　standpoint of the flash rate temporal variation. This section explores the mean values of

227　　storm attributes derived from WDSS-II. As Fig. 4 demonstrates, the LJ1 clusters exhibit

228　　a longer lifespan than the respective LJ0, and this observation is consistent throughout

229　　the three lightning detection systems and all α and FRT values. For example, for α=2.0

230　　and FRT=15 f m^{-1}, the average lifespan is 80 min, whereas the respective LJ0 lifespan is

231   approximately 35 min. Similar behavior is evident for the mean flash rate (normalized

232   by the cluster's footprint area, f m^{-1} km^{-2}, Fig. 5), MESH (Fig. 6) and VIL (Fig. 7)

233   values.

234   In particular, Fig. 5 indicates that on average, the LJ1 clusters exhibit ~4-5 times

235   higher flash rates than the respective LJ0. For instance, the average LJ1 flash rates for α

236   =2.0 and FRT=15 f m^{-1} are ~0.054 f m^{-1} km^{-2} as opposed to ~0.015 f m^{-1} km^{-2} for the

237   LJ0, an observation that is also consistent across all networks. In turn, the MESH values

238   for the LJ1 clusters range from ~11-18 mm whereas the LJ0 corresponding values range

239   from ~6.5-10 mm (Fig. 6). Likewise, the mean values of VIL are ~ 18 kg m^{-2} for the

240   LJ0 and ~25 kg m^{-2} for the respective LJ1 (Fig. 7). As also highlighted in Section 3.2,

241   higher flash rates, larger MESH and VIL values (Figs. 5-7) are found with increasing α

242   and FRT thresholds. One could argue that it would be expected to have higher

243   magnitudes of weather severity proxies (e.g., MESH, VIL etc.) with higher flash rates.

244   Nevertheless, the previous results also suggest that it is not only the flash rate (i.e., FRT)

245   that exhibits a fundamental physical tie to storm intensity but also its temporal evolution

246   (i.e., α). The above results are also in agreement with the findings by Rudlosky and

247   Fuelberg (2013).

248   *3.4 LJ strength and storm decay time*

249   The results shown in Fig. 4 support that the LJ1 clusters with larger α and FRT

250   relate to storms with longer durations (Fig. 4). Approaching this from a different

251   perspective one can raise the following question: "Does the strength of the final LJ

252 occurrence relate to the remaining lifespan of the cluster?" To address this question the

253 time elapsed from the last LJ occurrence to the last time-step that a cluster is tracked is

254 computed in minutes. Arguably, the results in Fig. 8 corroborate that both α and FRT

255 play a role in the storms' remaining duration which shows to increase from around 30-

256 35 min for LJ1 of α = 1.0 and FRT=10 f m^{-1} to over 45-60 min for higher α and/or FRT

257 values.

258 **4. Conclusions**

259   The observations herein indicate that the presence of LJ has implications for the

260 storm dynamics, intensity and evolution. The e-folding times are lower for the LJ1

261 clusters. For example the e-folding times for the LJ1 at α =2.0 and FRT=15 f m^{-1} are

262 computed as ~12 min for LMA, 12.7 min for the ENTLN, and 11.5 min for the NLDN.

263 Conversely, the e-folding times for the LJ0 for the same α and FRT values are

264 consistently less than ~4.0 min for all three lightning detection systems. Through the

265 enhanced updraft hypothesis, these findings indicate that the presence of a LJ signals the

266 storm's ability to sustain convection.

267   The study also documents that LJ1 clusters last longer and exhibit higher flash

268 rates (area-normalized), MESH and VIL values, further corroborating previous studies

269 that also suggest that the temporal total lightning variability is a dependable proxy for

270 severe weather risk assessment (Williams 2001; Schultz et al. 2009; 2011; Rudlosky and

271 Fuelberg 2013). In addition, the MESH values for the LJ1 clusters range from ~11-18

272 mm whereas the LJ0 respective values range from ~6.5-10 mm (Fig. 5). The mean

273   values of VIL are ~ 18 kg m^{-2} for the LJ0 and ~25 kg m^{-2} for the LJ1 clusters.

274   The results throughout this analysis consistently suggest that there is no

275   redundancy in the role of α and FRT in the LJ numerical implementation. This is shown

276   by the increasing magnitudes of the implicated variables (e.g. e-folding time, MESH,

277   flash rate etc., see Fig.2-7) for LJ1 clusters increase as both α and FRT values also

278   increase. Finally, the study offers further evidence that the presence and temporal

279   coincidence of a LJ could be viewed as a proxy of the storm's expected dissipation.

280   Typically, these values range between 20-60 min depending on the LJ strength with

281   stronger jumps indicating more time until storm decay.

282   Ongoing efforts explore the value of the LJ as a component in the operational

283   severe weather watch/warnings issuance (Schultz et al. 2014). The upcoming Geo-

284   stationary Lightning Mapper (GLM) onboard the GOES-R mission (Goodman et al.

285   2013) will provide continuous monitoring of total lightning activity across the Western

286   Hemisphere. GLM will provide even greater detail on the linkage between temporal

287   lightning variability and the storm evolution over areas where currently related

288   information, including radar, is limited or nonexistent. Importantly, GLM will provide

289   continuous coverage of total lightning over a large domain to evaluate this study on the

290   global scale.

4. **References**

Amburn, S., and P. Wolf, 1996: VIL Density as a Hail Indicator. 18th Conference on
   Severe Local Storms. San Francisco, CA, Amer. Meteor. Soc., 581-585.

Bowerman, B. L., and O'Connell, R. T., 1979: *Time Series and Forecasting*, Duxbury Press, North Scituate, Massachusetts.

Bruning, Eric C., Donald R. MacGorman, 2013: Theory and Observations of Controls on Lightning Flash Size Spectra. *J. Atmos. Sci.*, **70**, 4012–4029.

313   Carey, L. D. and S. A. Rutledge, 2000: On the relationship between precipitation

314   and lightning in tropical island convection: A C-band polarimetric radar study.

315   Monthly Weather Review, 128, 2687–2710.

316   Carey, L. D., W. A. Petersen, and C. J. Schultz, 2009: A statistical framework for

317   the development and evaluation of a lightning jump algorithm. Preprints, Fourth

318   Conference on the Meteorological Applications of Lightning Data, Phoenix, AZ,

319   Amer. Meteor. Soc. d

320   Chronis T., Williams E, Anagnostou E., Walt Petersen, 2007: Lightning as a precursor

321   of tropical cyclogenesis, Eos Trans. AGU, 88(40), 397, 10.1029/2007EO400001.

322

323   Cintineo, L. J., Michael J. Pavolonis, Justin M. Sieglaff, Daniel T. Lindsey, 2014:

324   An Empirical Model for Assessing the Severe Weather Potential of Developing

325   Convection

326

327   Cintineo, L. J., Travis M. Smith, Valliappa Lakshmanan, Harold E. Brooks, Kiel

328   L. Ortega, 2012: An Objective High-Resolution Hail Climatology of the

329   Contiguous United States. Wea. Forecasting, 27, 1235–1248. doi:

330   http://dx.doi.org/10.1175/WAF-D-11-00151.1

331

332   Cummins, K. L., E. A. Bardo, W. L. Hiscox, R. B. Pyle, and A. E. Pifer, 1995:

333   NLDN '95: A combined TOA/MDF technology upgrade of the U.S. National

334   Lightning Detection Network, 1995: International Aerospace and Ground

335   Conference on Lightning and Static Electricity, Williamsburg, Virginia, 26-28

336   Sept 1995.

337

338   Cummins, K., E. P. Krider and M. Malone, 1998: The U.S. National Detection

339   network and applications of cloud-to-ground lightning data by electric power

340   utilities, IEEE Trans. on Electromagnetic Compatibility, Vol. 40, no. 4.

341
342
343   Cummins, K. L., J. Cramer, C. Biagi, E. P. Krider, J. Jerauld, M. Uman, and V.

344   Rakov, 2006: The U.S. National Lightning Detection Network: Post-upgrade

345   status. Second Conference on Meteorological Applications of Lightning Data,

346   Atlanta, Georgia, American Meteorological Society.

347

348   Cummins, K. L., and M. J. Murphy, 2009: An overview of lightning locating

349   systems: History, techniques, and data uses, with an in-depth look at the U.S.

350   NLDN. IEEE Trans. on Electromagnetic Compatibility, 51, 3, 499- 518.

351

352 Deierling, W., and W. A. Petersen, 2008: Total lightning activity as an indicator

353 of updraft characteristics, J. Geophys. Res., 113, D16210,

354 doi:10.1029/2007JD009598.

355

356 Emersic, C. and C.P.R. Saunders, 2010: Further laboratory investigations into the

357 relative diffusional growth rate theory of thunderstorm electrification. Atmos.

358 Res., 98, doi:10.1016/j.atmosres.2010.07.011

359

360 Gatlin, P., Goodman, S.J., 2010: A total lightning trending algorithm to identify

361 severe thunderstorms. J. Atmos. Ocean. Technol. 27, 3–22.

362

363 Goodman, S. J., D. E. Buechler, P. D. Wright, and W. D. Rust, 1988: Lightning

364 and precipitation history of a microburst-producing storm. Geophys. Res. Lett.,

365 15, 1185–1188.

366 Goodman, S. J., R. Blakeslee, H. Christian, W. Koshak, J. Bailey, J. Hall, E.

367 McCaul, D. Beuchler, C. Darden, J. Burks, T. Bradshaw, P. Gatlin, 2005: The

368 North Alabama Lightning Mapping Array: Recent severe storm observations and

369 future prospects. *Atmos. Res.,* **76**, 423-437.

370

371 Goodman S, Blakeslee R, Koshak W, Mach D, Bailey J, Buechler D, Carey L, Schultz

372 C, Bateman M, Jr. E, et al. *The GOES-R Geostationary Lightning Mapper (GLM)*.

373 Atmospheric Research. 2013;125-126 34-49.

374

375 Greene, D. R., and R. A. Clark, 1972: Vertically integrated liquid water- A new

376 analysis tool. Mon. Wea. Rev., 100, 548-552

377

378

379

380 Koshak, W. J., R. J. Solakiewicz, R. J. Blakeslee, S. J. Goodman, , H. J. Christian,

381 J. M. Hall, J. C. Bailey, E. P. Krider, M. G. Bateman, D. J. Boccippio, D. M.

382 Mach, E. W. McCaul, M. F. Stewart, D. E. Buechler, W. A. Petersen, D. J. Cecil,

383 2004: North Alabama Lightning Mapping Array (LMA): VHF source retrieval

384 algorithm and error analyses, *J. Atmos. Oceanic Technol*., 21, 543-558.

385

386 Keene, K. M., P. T. Schlatter, J. E. Hales, and H. Brooks, 2008: Evaluation of

387 NWS watch and warning performance related to tornadic events. Preprints, 24th

388 Conf. on Severe Local Storms, Savannah, GA, Amer. Meteor. Soc., P3.19.

389 Krehbiel, P. R., 2008: The DC Lightning Mapping Ar- ray. Preprints, Third

390 Conference on Meteorological Ap- plications of Lightning Data, New Orleans,

391 LA, USA, American Meteorological Society. 3.2.

392 Krehbiel, P. R., 2008: The DC Lightning Mapping Array. Preprints, Third Conf.

393 on Meteorological Applications of Lightning Data, New Orleans, LA, Amer.

394 Meteor.   Soc.,   3.2.   [Available   online   at

395 http://ams.confex.com/ams/pdfpapers/129095.pdf.]

396 Lakshmanan, V., and T. Smith, 2009: Data mining storm attributes from spatial

397 grids. J. Atmos. Oceanic Technol., 26, 2353–2365.

398

399 Lakshmanan, V., K.Hondl, and R.Rabin, 2009: An efficient, general-purpose

400 technique for identifying storm cells in geospatial images,' J. Ocean. Atmos.

401 Tech., vol.26, no.3, pp.523-37.

402

403 Lakshmanan, V., T. Smith, G. J. Stumpf, and, K. Hondl, 2007: The Warning

404 Decision Support System–Integrated Information. Wea. Forecasting, 22, 596–612.

405   Lang, T. J., and Rutledge, S. A., 2002: Relationships between convective

406 storm kinematics, precipitation, and lightning. Mon. Wea. Rev., 130: 2492–2506.

407

408 Liu C., and Heckman S., 2011: Using Total Lightning Data and Cell Tracking in

409 Severe Weather Prediction, 91st AMS meeting.

410 MacGorman, D. and C. D. Morgenstern, 1998: Some characteristics of cloud to ground

411 lightning in mesoscale convective systems, J. Geophys. Res., 103, D12, 14,011-14,023.

412

413 MacGorman, D.R., Rust, W.D., Schuur, T.J., Biggerstaff, M.I., Straka, J.M., Ziegler,

414 C.L., Mansell, E.R., Bruning, E.C., Kuhlman, K.M., Lund, N.R., Biermann, N.S., Payne,

415 C., Carey, L.D., Krehbiel, P.R., Rison, W., Eack, K.B., Beasley, W.H., 2008. TELEX:

416 The Thunderstorm Electrification and Lightning Experiment. Bull. Am. Meteorol. Soc.

417 89, 997–1013.

418

419 McCaul, E. W., J. Bailey, J. Hall, S. J. Goodman, R. Blakeslee, and D. E. Buechler,

420 2005: A flash clustering algorithm for North Alabama Lightning Mapping Array data.

421 Preprints, *Conf. on Meteorological Applications of Lightning Data,* San Diego, CA,

422 Amer. Meteor. Soc., 5.2. [Available online at http://ams.confex.com/ams/

423 Annual2005/techprogram/paper_84373.htm].

424 Murphy, M. J. and A. Nag, 2014: Enhanced cloud lightning performance of the U.S.

425 National Lightning Detection Network following the 2013 upgrade, 23rd International

426 Lightning Detection Conference & 5th International Lightning Meteorology Conference,

427 18-21 March, Tucson, Arizona.

428

429   Petersen, W. A., H. J. Christian, and S. A. Rutledge, 2005: TRMM observations

430   of the global relationship between ice water content and lightning. Geophys. Res.

431   Lett., 32, doi: 10.1029/2005GL023236.

432   Scott D. Rudlosky, S D., and Henry E. Fuelberg, 2010: Pre- and Postupgrade Distributions of NLDN
433   Reported Cloud-to-Ground Lightning Characteristics in the Contiguous United States. *Mon. Wea. Rev.*,
434   **138**, 3623ea. Re doi: http://dx.doi.org/10.1175/2010MWR3283.1
435

436   Rudlosky, Scott D., and Henry E. Fuelberg. 2013: Documenting Storm Severity in

437   the Mid-Atlantic Region Using Lightning and Radar Information, Monthly

438   Weather Review 141, no. 9: 3186-3202.

439

440   Saunders, C. P. R., 1993: A Review of Thunderstorm Electrification Processes. J.

441   Appl. Meteor., 32, 642–655.

442   Saunders, C. P. R., H. Bax-Norman, C. Emersic, E. E. Avila, and N. E.

443   Castellano, 2006: Laboratory studies of the effect of cloud conditions on

444   graupel/crystal charge transfer in thunderstorm electrification. Quart. J. Roy.

445   Meteor. Soc., 132, 2653-2673.

446   Schultz, C. J. L.D. Carey, E. V. Schultz, R. J. Blakeslee and S. J. Goodman,

447   2014: Physical and dynamical linkages between lightning jumps and storm

448   conceptual models. Conference Proceedings 15th International Conf. on

449   Atmospheric Electricity. Norman, OK.

450   Schultz, C. J., W. A. Petersen, L. D. Carey, 2011: Lightning and Severe

451   Weather: A Comparison between Total and Cloud-to-Ground Lightning Trends.

452   Wea. Forecasting, 26, 744–755.

453   Schultz, C. J., W. A. Petersen, and L. D. Carey, 2009: Preliminary

454   development and evaluation of lightning jump algorithms for the real-time

455   detection of severe weather. J. Appl. Meteor. Climatol., 48, 2543–2563.

456   Shafer, Mark A., Donald R. MacGorman, Frederick H. Carr, 2000: Cloud-to-

457   Ground Lightning throughout the Lifetime of a Severe Storm System in

458   Oklahoma. Mon. Wea. Rev., 128, 1798–1816.

459   Stumpf, G.J., T. M. Smith and J. Hocker, 2004: New hail diagnostic

460   parameters derived by integrating multiple radars and multiple sensors. Preprints,

461   22nd Conf. on Severe Local Storms, Hyannis, MA, Amer. Meteor. Soc., CD-

462   ROM, P7.8.

463   Uman, 1987: The Lightning Discharge, Academic Press, pp. 183

464   Takahashi, T., 1978: Riming electrification as a charge generating mechanism

465   Thomas, R. J., P. R. Krehbiel, W. Rison, S. J. Hunyady, W. P. Winn, T. Hamlin,

466   and J. Harlin, 2004: Accuracy of the light- ning mapping array. J. Geophys. Res.,

467   109, D14207, doi:10.1029/ 2004JD004549.

468 Thomas, R., P. Krehbiel, W. Rison, J. Harlin, T. Hamlin, and N. Campbell, 2003:

469 The LMA flash algorithm. Proc. 12th Int. Conf. on Atmospheric Electricity,

470 Versailles, France, In- ternational Commission on Atmospheric Electricity, 655–

471 656.

472 Trapp, R. J., D. M. Wheatly, N. T. Atkins, and R. W. Przybylinkski, 2006:

473 Buyer beware: Some words of caution on the use of severe wind reports in

474 postevent assessment and research. Wea. Forecasting, 21, 408–415.

475 Vonnegut, B., 1963: Some facts and speculation concerning the origin and

476 role of thunderstorm electricity. Severe Local Storms, Meteor. Monogr., Amer.

477 Meteor. Soc., 224–241.

478 water on thunderstorm charging, J. Geophys. Res., 96, 11,007–11,017,

479 doi:10.1029/91JD00970.

480 Wea.Forecasting. In Press. http://journals.ametsoc.org/doi/pdf/10.1175/WAF-D-

481 13-00113.1

482 Williams, E. R., 1985: Large scale charge separation in thunderclouds. J.

483 Geophys. Res., 90, 6013–6025.

484 Williams, E. R., Bob Boldi, Anne Matlin, Mark Weber, Steve Hodanish,

485 Dave Sharp, Steve Goodman, Ravi Raghavan, Dennis Buechler, 1999: The

486   behavior of total lightning activity in severe Florida thunderstorms, Atmospheric

487   Research, Volume 51, Issues 3–4, Pages 245-265.

488   Williams, E.R., 2001: The Electrification of Severe Storms, Chapter 13 in Severe

489   Convective Storms, Ed., C.A. Doswell, III, Meteorological Monograph, Vol. 28,

490   No. 50, 527-561.

491   Witt, A., M. D. Eilts, G. J. Stumpf, J. T. Johnson, E. D. Mitchell, and K. W.

492   Thomas, 1998: An enhanced hail detection algorithm for the WSR-88D. Wea.

493   Forecasting, 13, 286-303.

494

495   **Figure Captions**

496   Figure 1: Tracked cluster that exhibits a problematic tracking (e.g. cluster entering the area with already high flash rates,

497   Fig.1a), a normal tracking (i.e. comply with both QC1 and QC2, Fig.1b), a LJ0 cluster (Fig.1c) and a LJ1 cluster (Fig.1d) of

498   comparable flash rates.

499

500   Figure 2: The identified number of LJ0/LJ1 clusters as a function of FRT (x-axis, $f\ m^{-1}$) and α (y-axis,), LMA-

501   a/b, ENTLN-c/d and NLDN-e/f

502   Figure 3: Mean e-folding time (min) for LJ0/LJ1, as a function of FRT (x-axis, $f\ m^{-1}$) and α (y-axis,), LMA-

503   a/b, ENTLN-c/d and NLDN-e/f

504

505   Figure 4: Mean life-span (min) for LJ0/LJ1, as a function of FRT (x-axis, $f\ m^{-1}$) and α (y-axis,), LMA-a/b,

506   ENTLN-c/d and NLDN-e/f

507   Figure 5: Mean area-normalized flash rate (f m^{-1} km^{-2}) for LJ0/LJ1, as a function of FRT (x-axis, f m^{-1}) and α
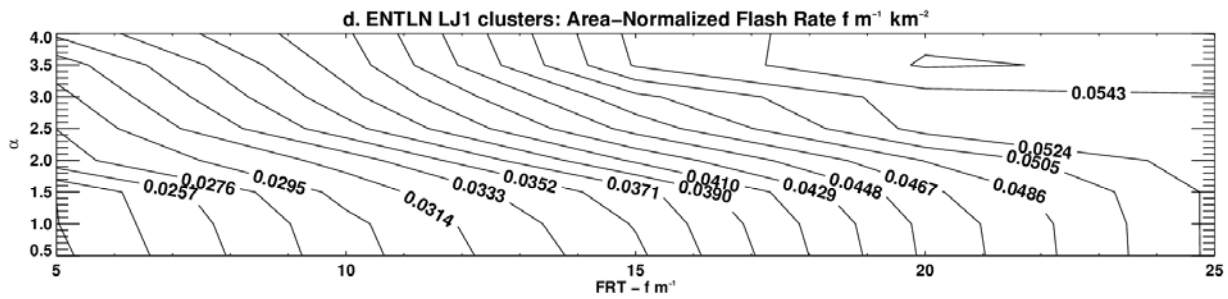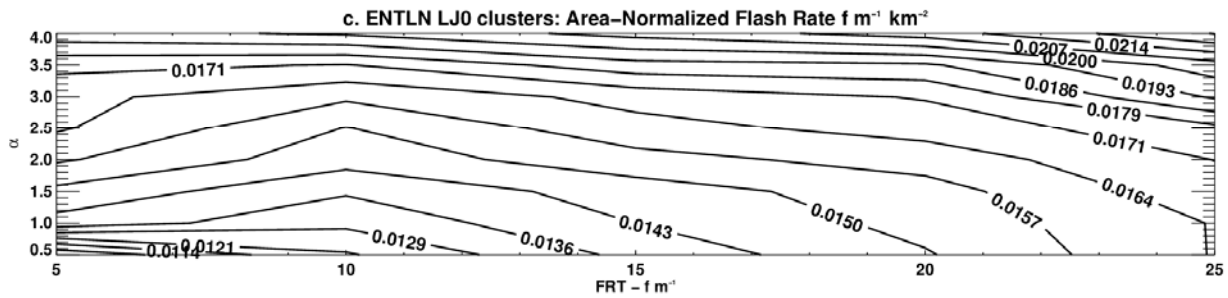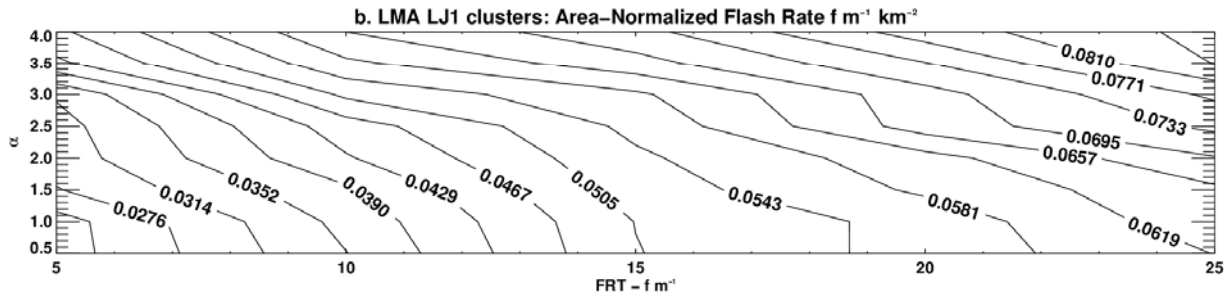
508   (y-axis,), LMA-a/b, ENTLN-c/d and NLDN-e/f

509   Figure 6: Mean MESH (mm) for LJ0/LJ1, as a function of FRT (x-axis, f m^{-1}) and α (y-axis,), LMA-a/b,

510   ENTLN-c/d and NLDN-e/f

511   Figure 7: Mean VIL (kg m^{-2}), for LJ0/LJ1 as a function of FRT (x-axis, f m^{-1}) and α (y-axis,), LMA-a/b,

512   ENTLN-c/d and NLDN-e/f

513   Figure 8: Time elapsed until the storm dissipation for LJ1 (min) (LMA-a, ENTLN-b and NLDN-c) as a

514   function of FRT (x-axis, f m^{-1}) and α (y-axis,).

515

516

517

518

519

520

521

522
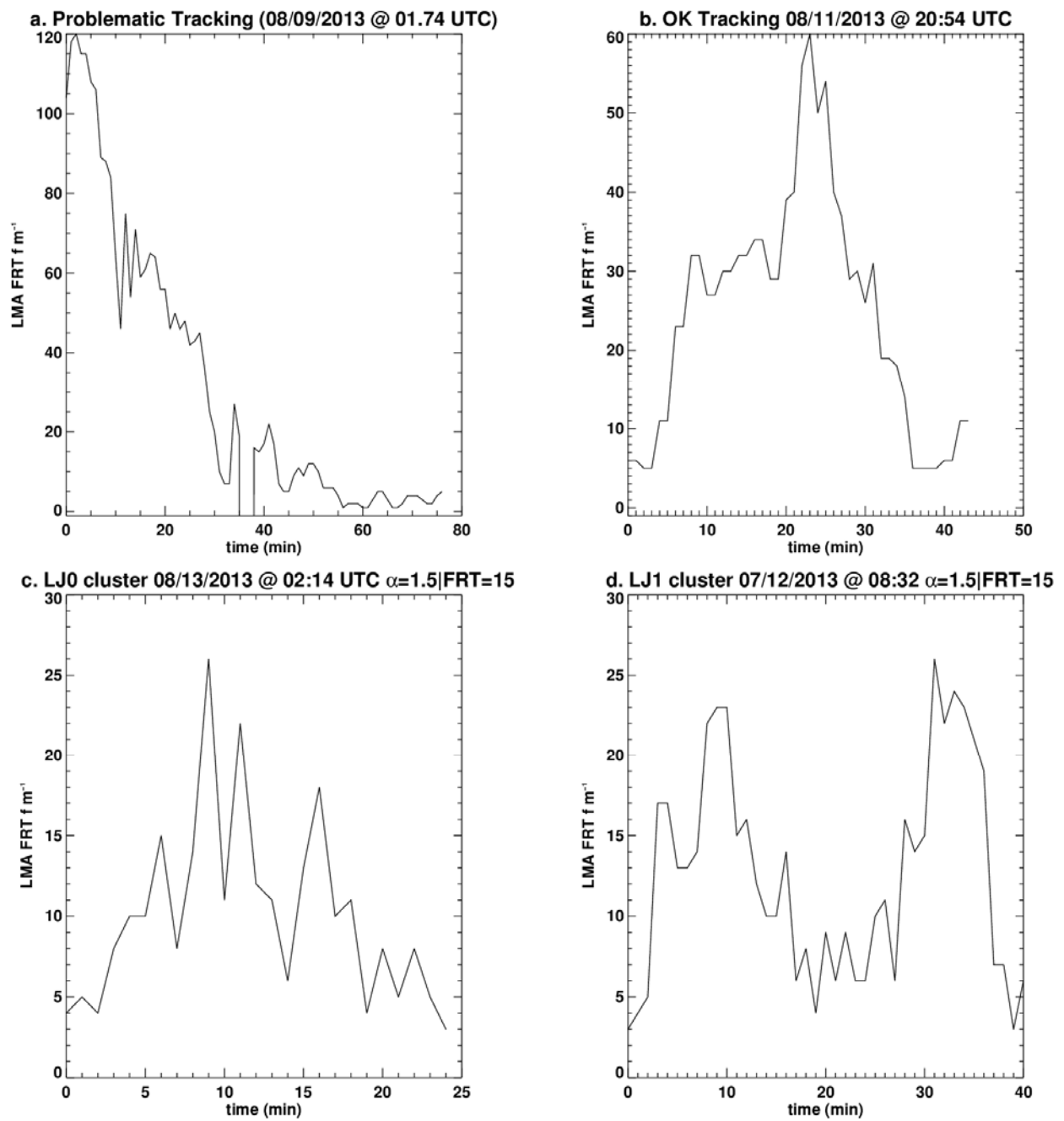
523

524

525   Figure 1: Tracked cluster that exhibits a problematic tracking (e.g. cluster entering the area with already high flash rates,

526   Fig.1a), a normal tracking (i.e. comply with both QC1 and QC2, Fig.1b), a LJ0 cluster (Fig.1c) and a LJ1 cluster (Fig.1d) of

527   comparable flash rates.

528

529

530

531

532

533

534

535

536

537

538

539

540

541

542

29 of 45
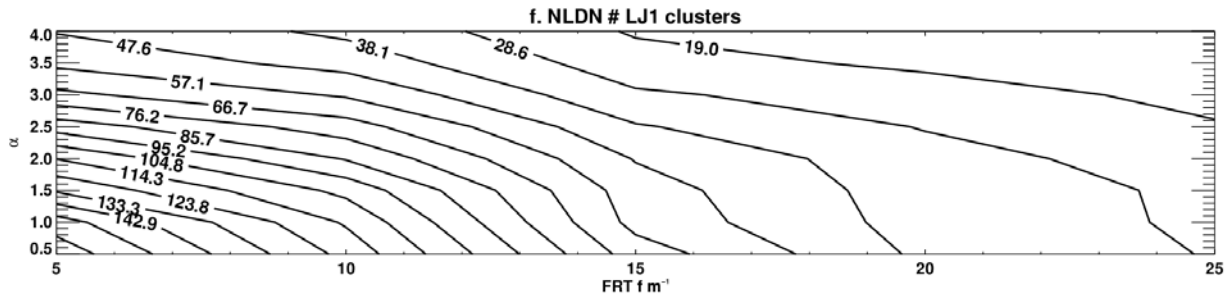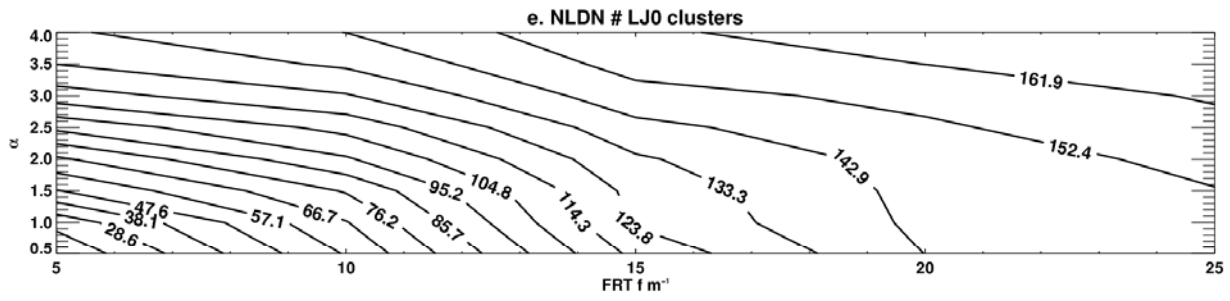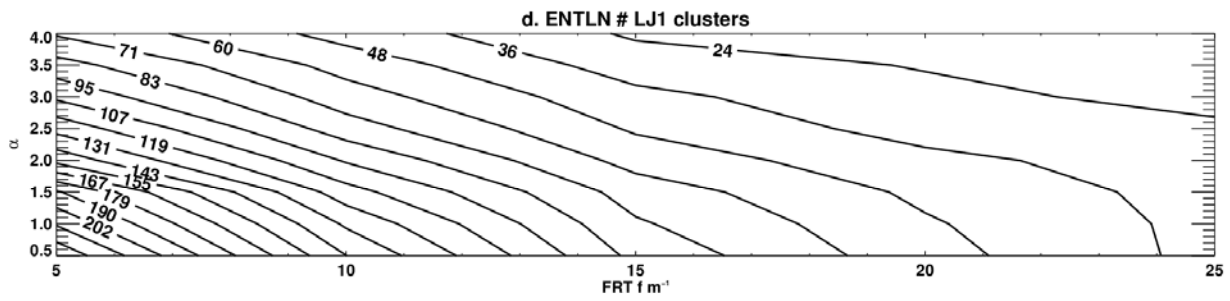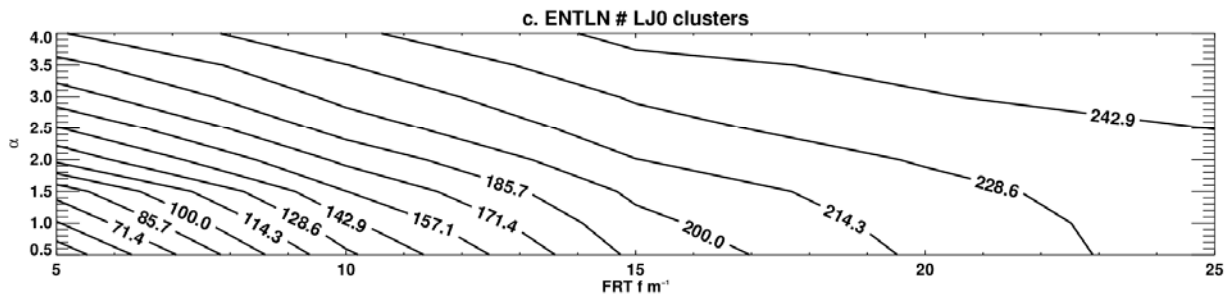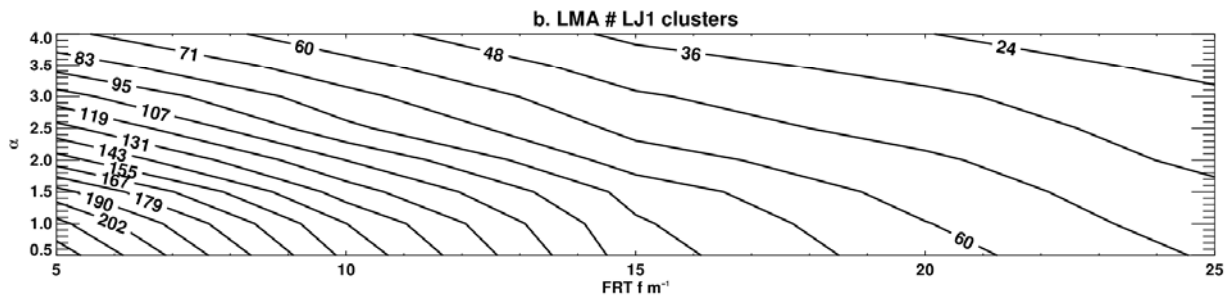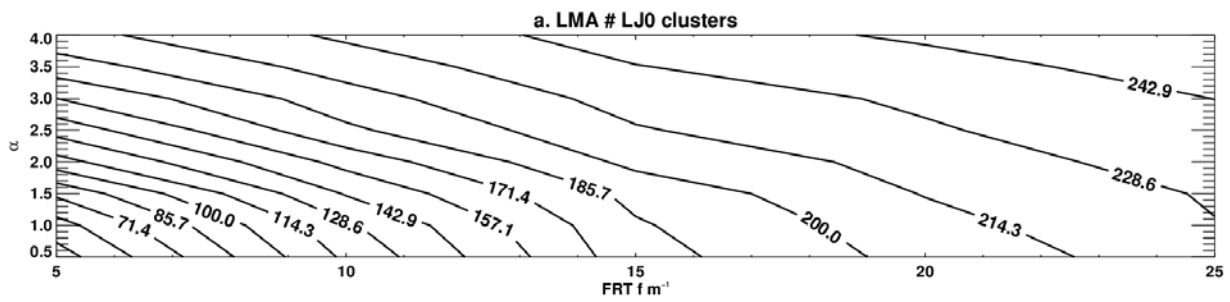
543   Figure 2: The identified number of LJ0/LJ1 clusters as a function of FRT (x-axis, $f\,m^{-1}$) and α (y-axis,), LMA-

544   a/b, ENTLN-c/d and NLDN-e/f

545

546

547

548

549

550

551

552

553

554

555

556

557

558

559

560

561

562

a. LMA LJ0 clusters: e_Folding Time (min)

b. LMA LJ1 clusters: e_Folding Time (min)

c. ENTLN LJ0 clusters: e_Folding Time (min)

d. ENTLN LJ1 clusters: e_Folding Time (min)

e. NLDN LJ0 clusters: e_Folding Time (min)

f. NLDN LJ1 clusters: e_Folding Time (min)

563
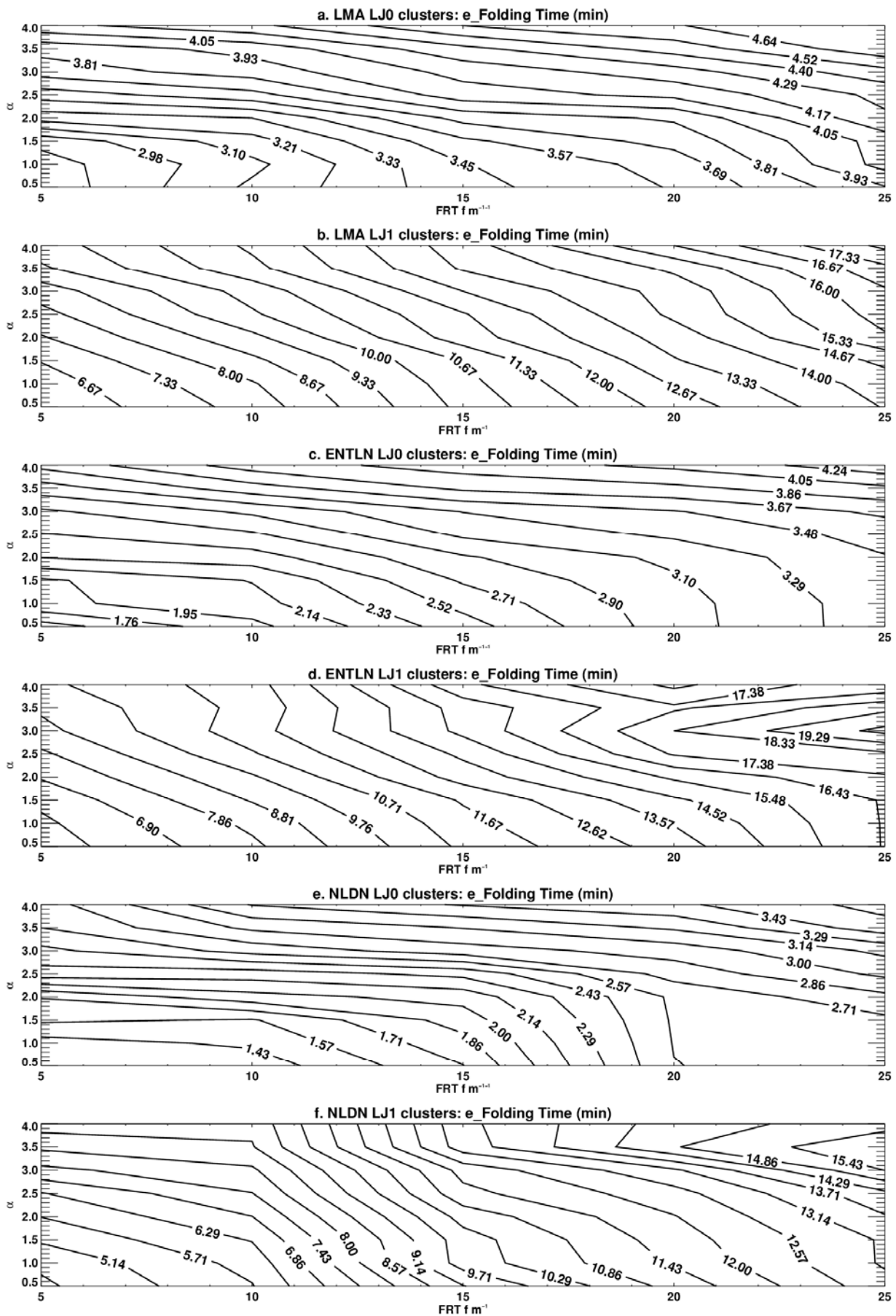
564   Figure 3: Mean e-folding time (min) for LJ0/LJ1, as a function of FRT (x-axis, f m^{-1}) and α (y-axis,), LMA-

565   a/b, ENTLN-c/d and NLDN-e/f

566

567

568

569

570

571

572

573
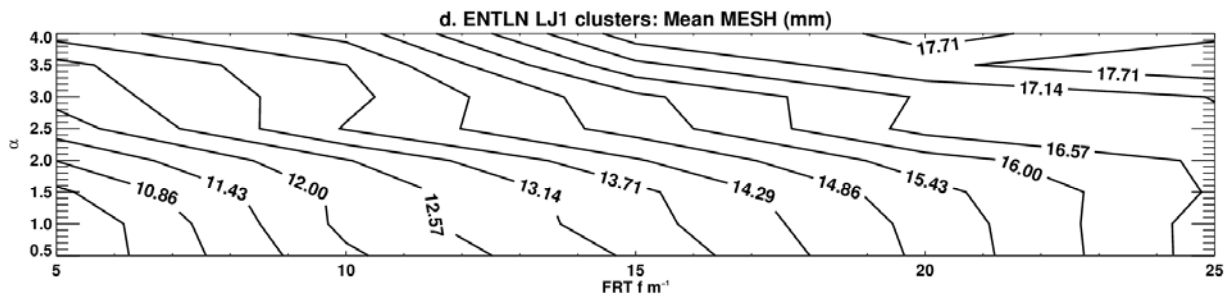
574

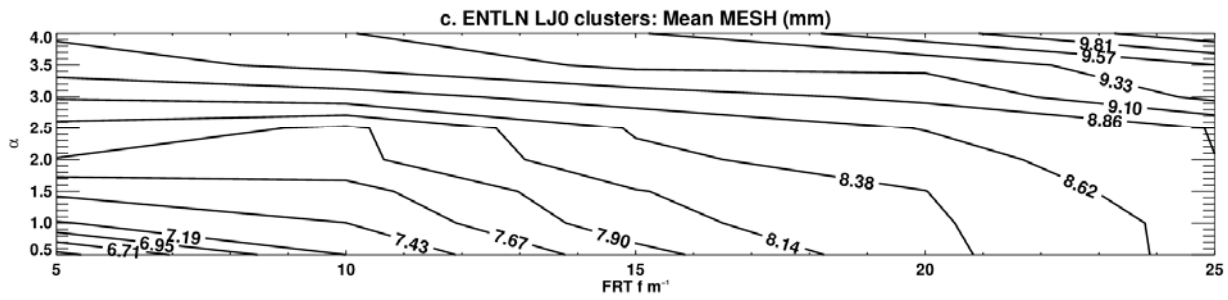575

576

577

578

579

580

581

582

583

584

a. LMA LJ0 clusters: Mean Lifespan (min)

b. LMA LJ1 clusters: Mean Lifespan (min)

c. ENTLN LJ0 clusters: Mean Lifespan (min)

d. ENTLN LJ1 clusters: Mean Lifespan (min)

e. NLDN LJ0 clusters: Mean Lifespan (min)

f. NLDN LJ1 clusters: Mean Lifespan (min)
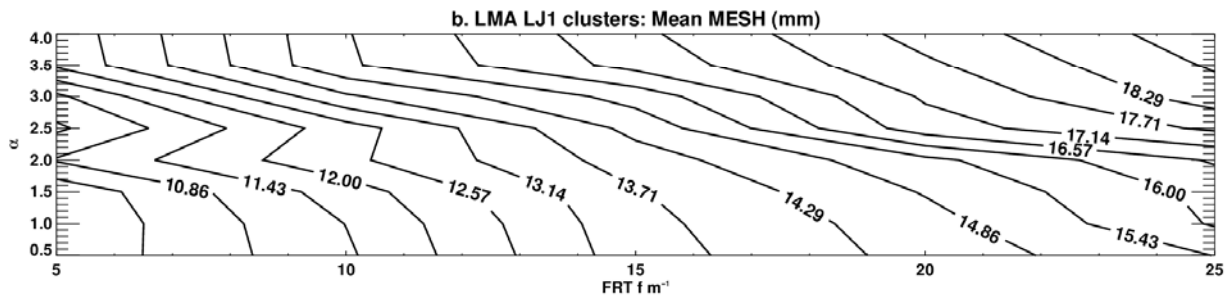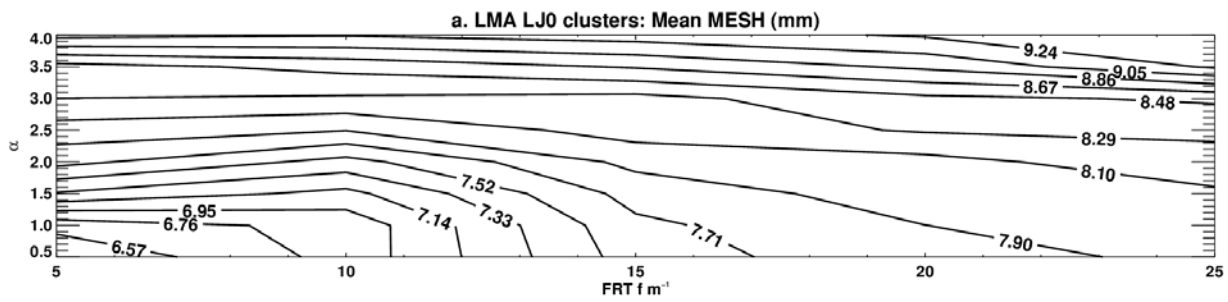
585
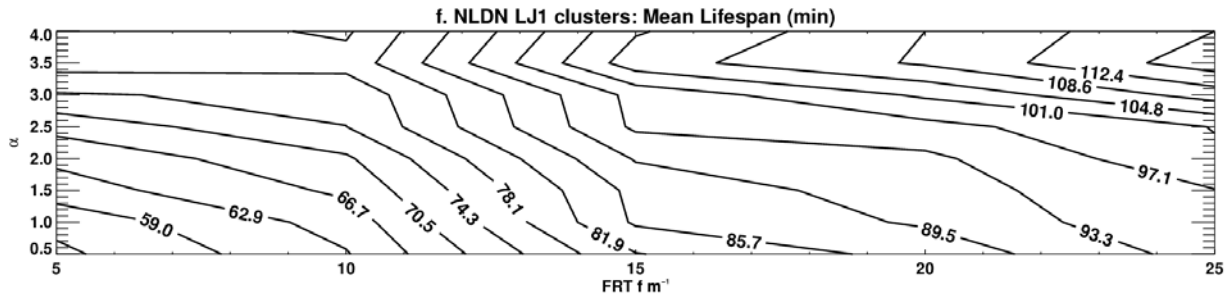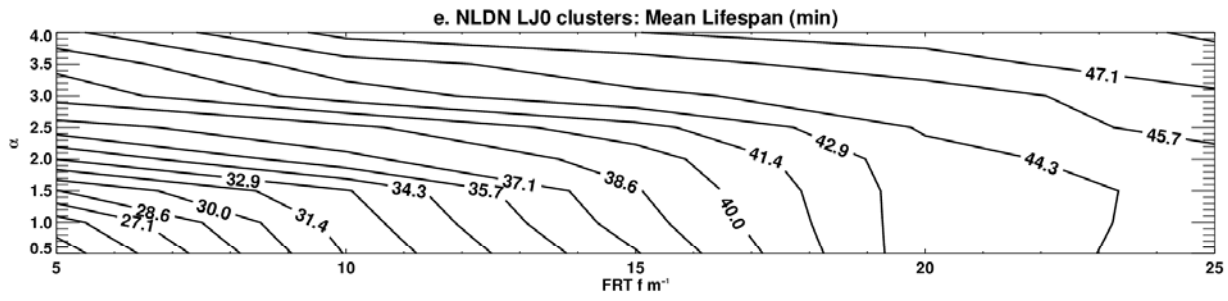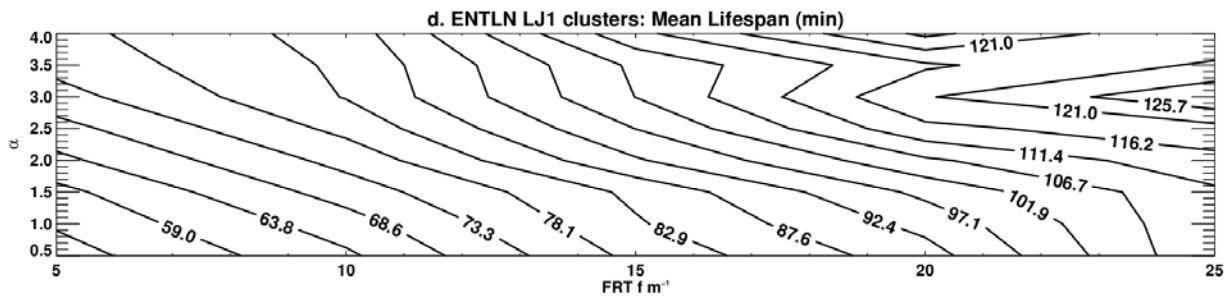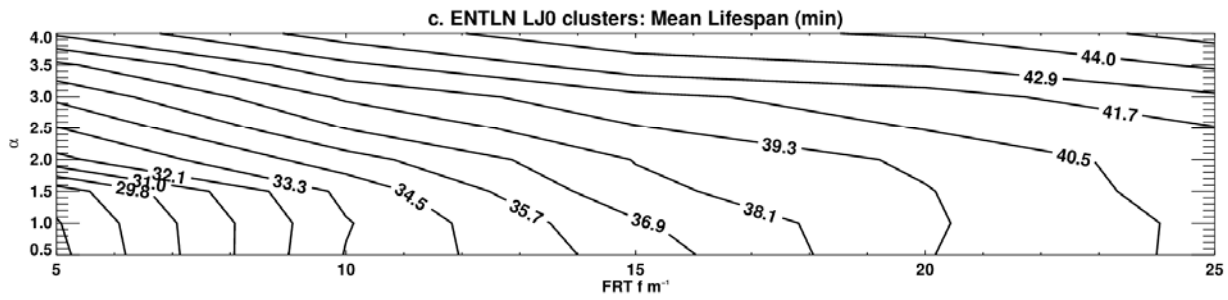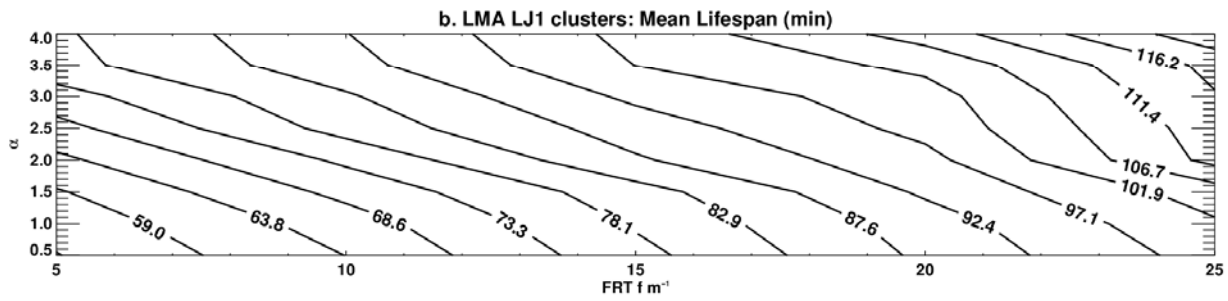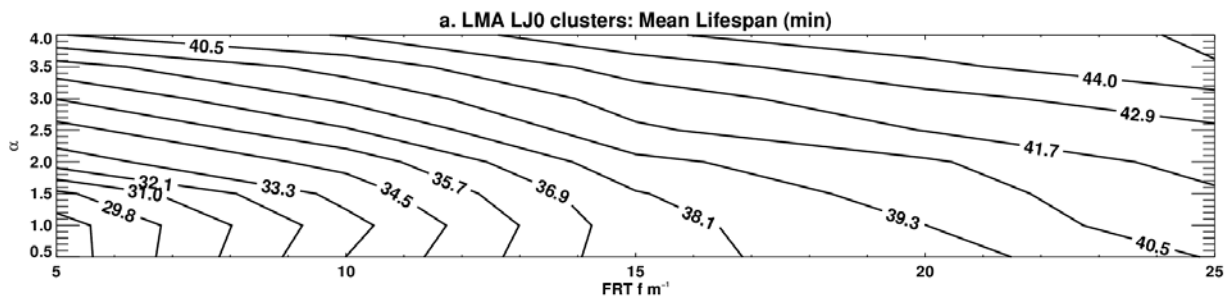
586   Figure 4: Mean life-span (min) for LJ0/LJ1, as a function of FRT (x-axis, f m^{-1}) and α (y-axis,), LMA-a/b,

587   ENTLN-c/d and NLDN-e/f

588

589

590

591

592

593

594

595

596

597
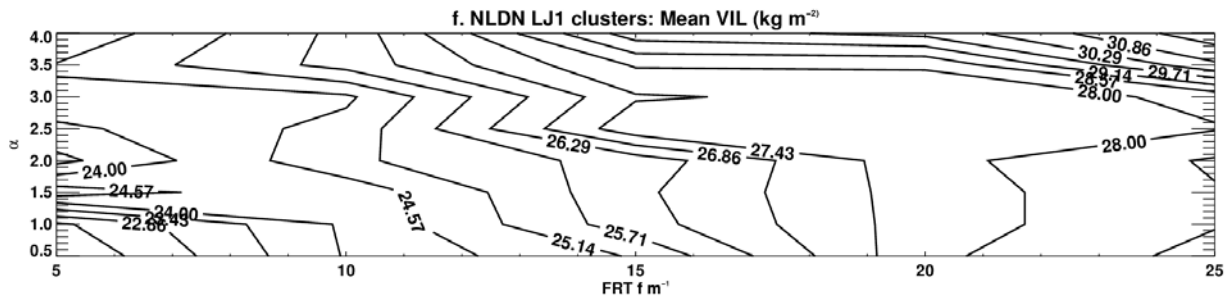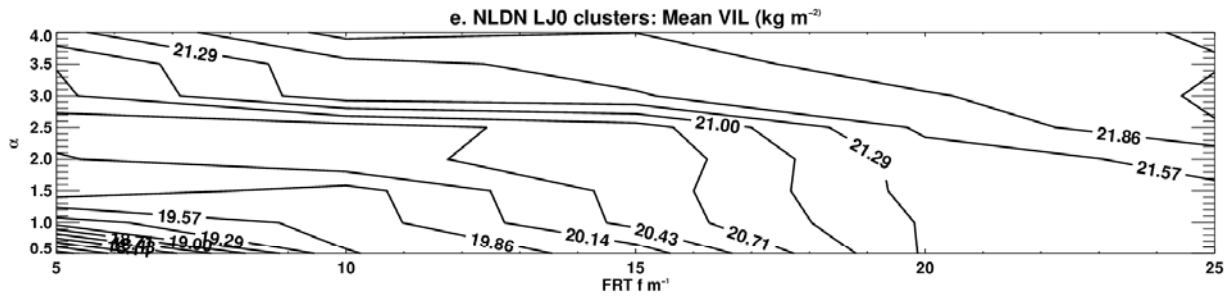
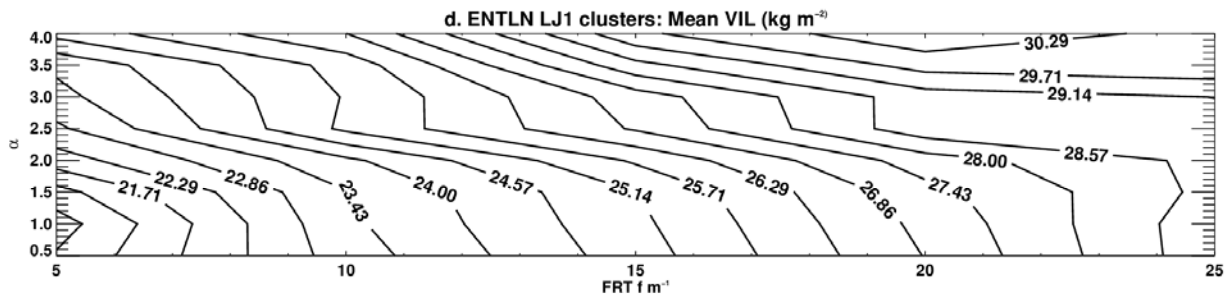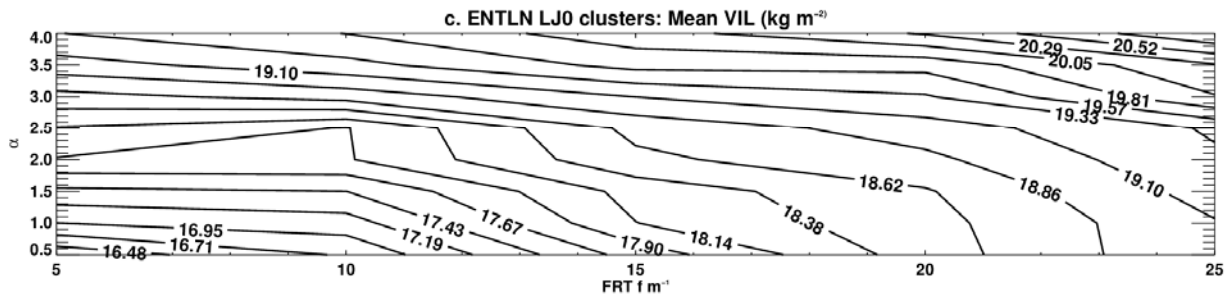598

599

600

601

602

603

604

605

a. LMA LJ0 clusters: Area–Normalized Flash Rate f m⁻¹ km⁻²

b. LMA LJ1 clusters: Area–Normalized Flash Rate f m⁻¹ km⁻²

c. ENTLN LJ0 clusters: Area–Normalized Flash Rate f m⁻¹ km⁻²

d. ENTLN LJ1 clusters: Area–Normalized Flash Rate f m⁻¹ km⁻²

e. NLDN LJ0 clusters: Area–Normalized Flash Rate f m⁻¹ km⁻²

f. NLDN LJ1 clusters: Area–Normalized Flash Rate f m⁻¹ km⁻²

606
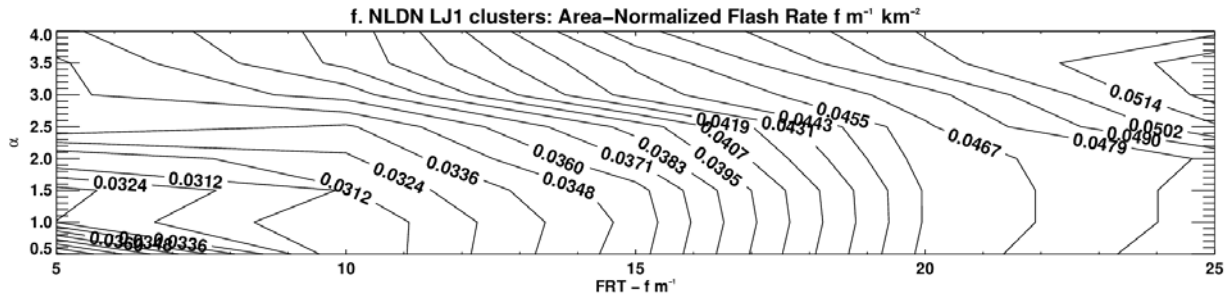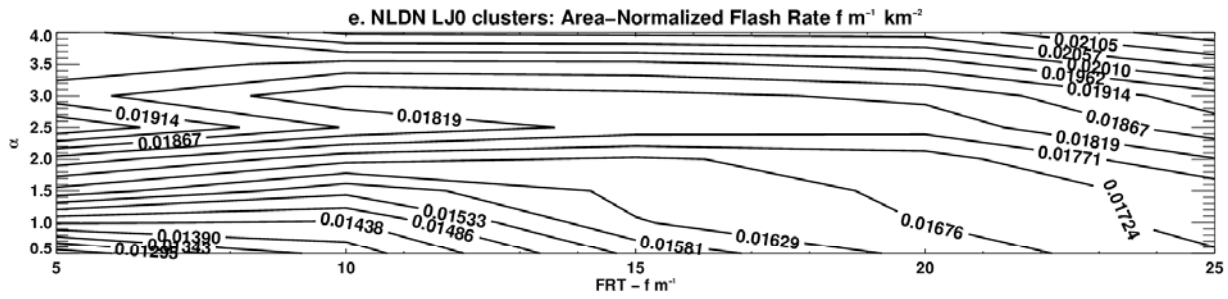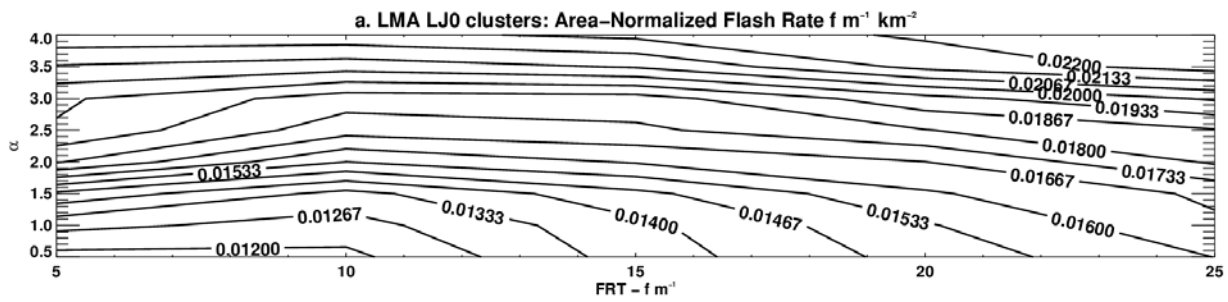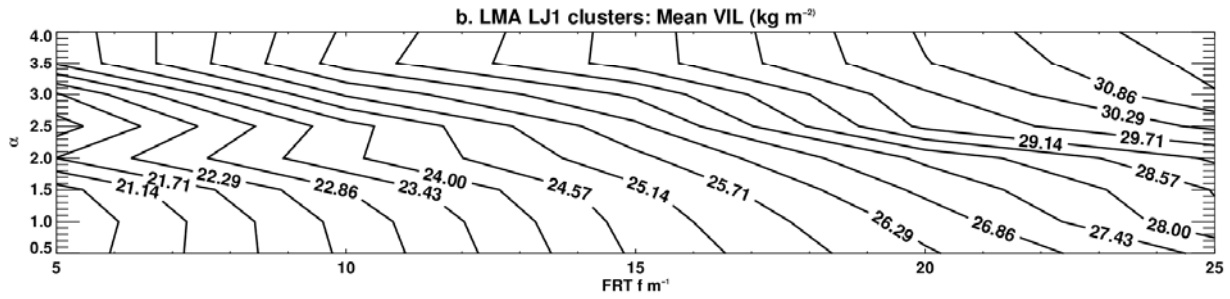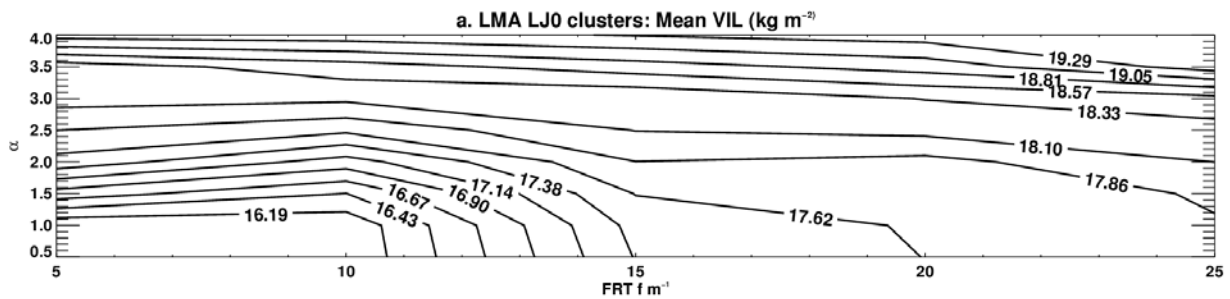
607   Figure 5: Mean area-normalized flash rate (f m^{-1} km^{-2}) for LJ0/LJ1, as a function of FRT (x-axis, f m^{-1}) and α

608   (y-axis,), LMA-a/b, ENTLN-c/d and NLDN-e/f

609

610

611

612

613

614

615

616

617

618

619

620

621

622

623

624

625

626

627

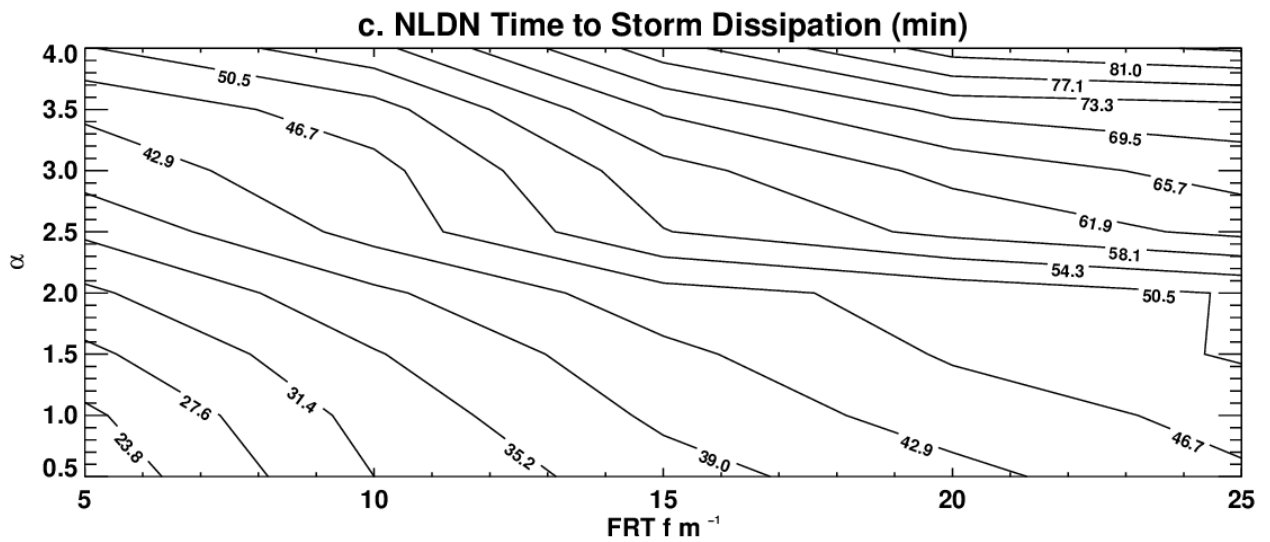628

a. LMA LJ0 clusters: Mean MESH (mm)

b. LMA LJ1 clusters: Mean MESH (mm)

c. ENTLN LJ0 clusters: Mean MESH (mm)

d. ENTLN LJ1 clusters: Mean MESH (mm)

e. NLDN LJ0 clusters: Mean MESH (mm)

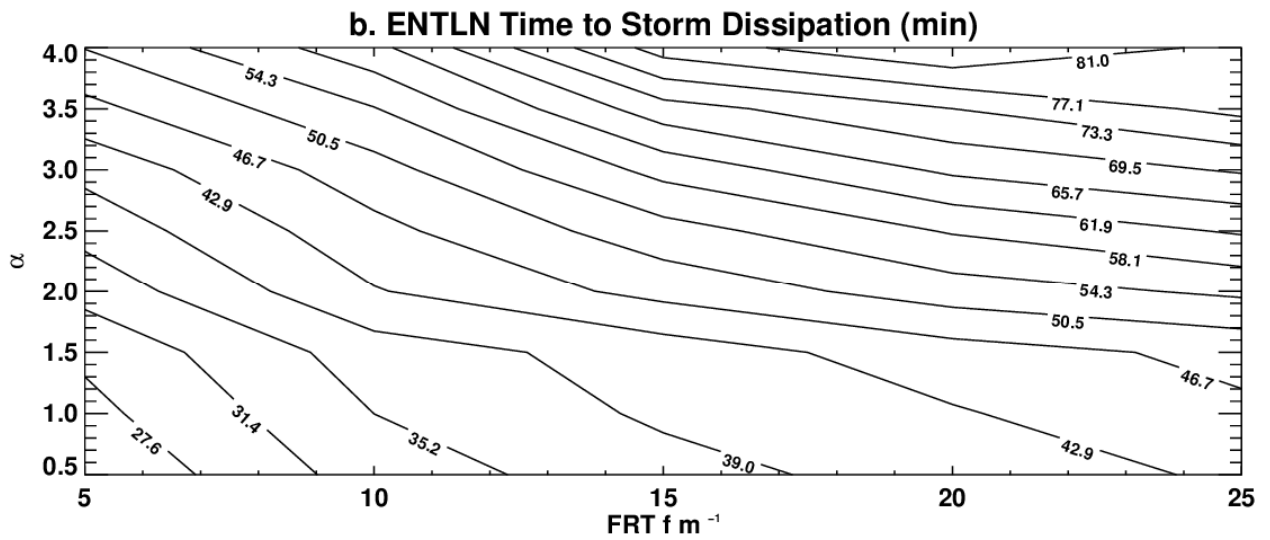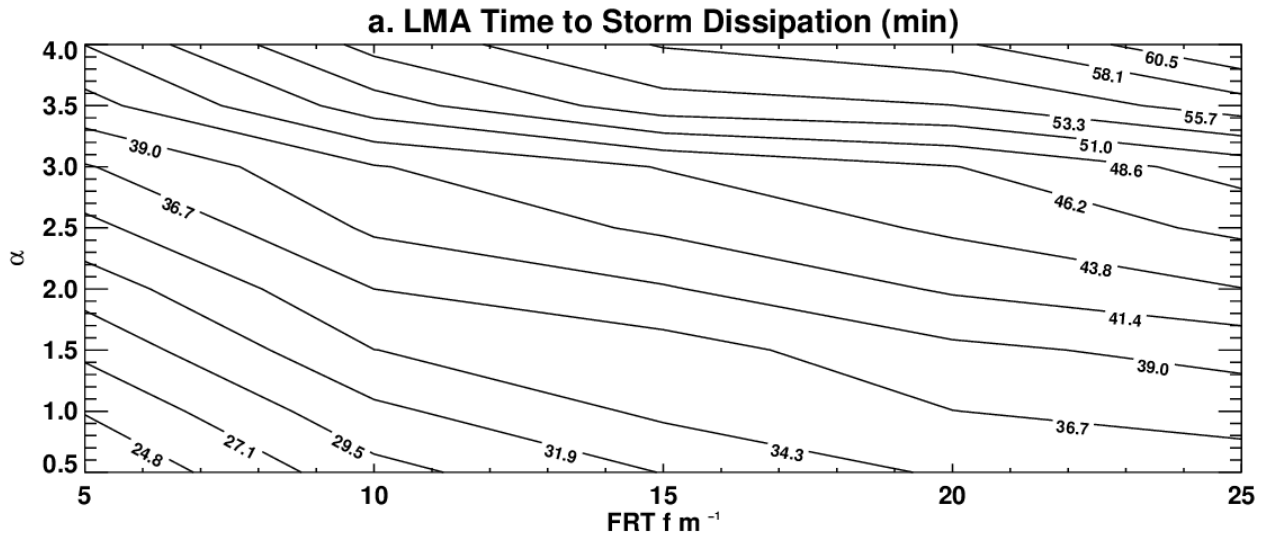f. NLDN LJ1 clusters: Mean MESH (mm)

629
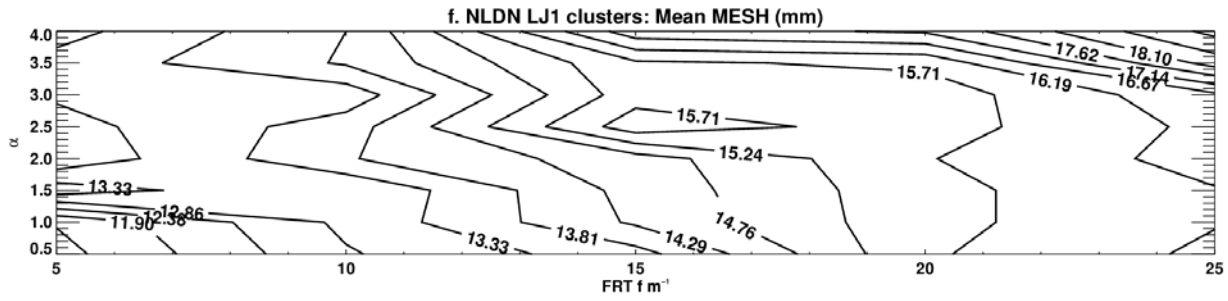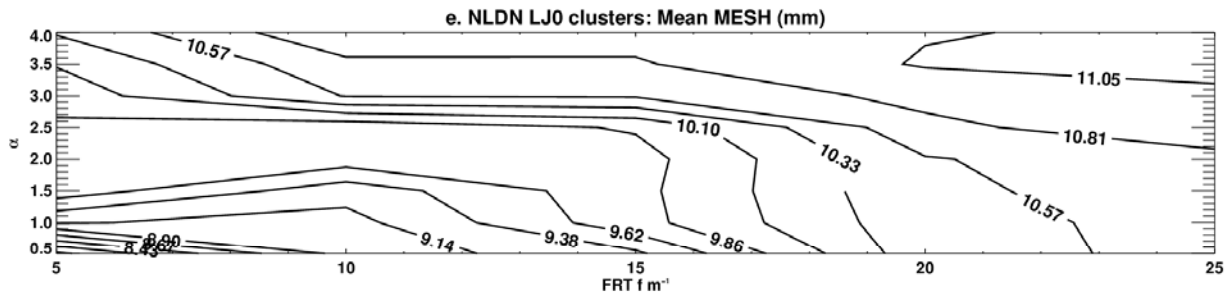
630 Figure 6: Mean MESH (mm) for LJ0/LJ1, as a function of FRT (x-axis, f m^{-1}) and α (y-axis,), LMA-a/b,

631 ENTLN-c/d and NLDN-e/f

632

633

634

635

636

637

638

639

640

641

642

643

644

645

646

647

648

649

a. LMA LJ0 clusters: Mean VIL (kg m^{-2})

b. LMA LJ1 clusters: Mean VIL (kg m^{-2})

c. ENTLN LJ0 clusters: Mean VIL (kg m^{-2})

d. ENTLN LJ1 clusters: Mean VIL (kg m^{-2})

e. NLDN LJ0 clusters: Mean VIL (kg m^{-2})

f. NLDN LJ1 clusters: Mean VIL (kg m^{-2})

650

651   Figure 7: Mean VIL (kg m^{-2}), for LJ0/LJ1 as a function of FRT (x-axis, f m^{-1}) and α (y-axis,), LMA-a/b,

652   ENTLN-c/d and NLDN-e/f

653

654

655

656

657

658

659

660

661

662

663

664

665

666

667

668

669

670

671

a. LMA Time to Storm Dissipation (min)

b. ENTLN Time to Storm Dissipation (min)

c. NLDN Time to Storm Dissipation (min)

672

43 of 45

673   Figure 8: Time elapsed until the storm dissipation for LJ1 (min) (LMA-a, ENTLN-b and NLDN-c) as a

674   function of FRT (x-axis, f m^{-1}) and α (y-axis,).

675

676

677

678

679

680

681

682

683

684

685

686

687

688

689

690

691

692

693